Self-amplitude-modulation of optical pulses in nonlinear dispersive fibers

M. J. Potasek and G. P. Agrawal
AT&T Bell Laboratories, Murray Hill, New Jersey 07974
(Received 23 October 1986; revised manuscript received 29 June 1987)

We consider propagation of optical pulses in the anomalous dispersive region of single-mode fibers after including the effects of Kerr-type nonlinearity. It is found that the pulse develops an internal structure with deep amplitude modulation. We show that this self-amplitude-modulation of pulses is related to the modulation instability of continuous-wave optical beams in nonlinear dispersive fibers. The initiation of this phenomenon does not require an external probe or spontaneous emission. Numerical results show that self-phase-modulation broadens the power spectrum enough to encompass the frequency at which self-amplitude-modulation provides the maximum gain. The amplification of these sidebands manifests as a breaking of the optical pulse into several subpulses. For negligible loss, the pulse breakup may also be viewed as the internal structure of a high-order soliton. However, modulation instability appears to provide a simpler interpretation and explains the features of numerical simulation and experiments.

I. INTRODUCTION

The study of nonlinear optical effects in silica fibers has been of considerable recent interest[1–17] and has led to new developments such as the soliton laser.[3] One of the widely studied nonlinear phenomena is self-phase-modulation (SPM) that has been successfully exploited for pulse compression in the picosecond regime.[9,11] One may expect that under certain conditions SPM should lead to self-amplitude-modulation (SAM) of optical pulses during their propagation inside the fiber. Indeed, the propagation of an intense, continuous-wave (cw) optical beam in a nonlinear dispersive fiber is inherently unstable in the anomalous dispersion regime, a phenomenon referred to as the modulation instability.[12–17] An experimental manifestation of modulation instability for cw beams has proven to be difficult, because of other competing nonlinear effects (such as stimulated Brillouin scattering). Recent experimental results,[15] showing a modulated envelope developing from an initially 100-ps-wide pulse, have been interpreted as arising from modulational instability. However, the depth of modulation was believed to be relatively small and the modulation was viewed as arising solely from spontaneous emission.

However, since the modulation-instability theory applies to only cw beams, some departure from its predictions is expected for the case of pulsed operation (pulse width ~ 100 ps). We have used numerical simulations to quantify the differences. A new result is related to the origin of the subpulse formation. Whereas spontaneous emission or an external probe is essential for the breakup of a cw beam, in the pulsed case spectral broadening occurring due to SPM can itself provide the input necessary for the initiation of subpulse structure. The numerical results presented here justify this interpretation. A recent experiment has also confirmed this interpretation.[18]

II. WAVE EQUATION

We consider the propagation of optical pulses in a polarization-conserving single-mode fiber and write the optical field in the form

$$E(r,t)=\hat{\mathbf{e}}U(\rho)A(z,t)\exp[-i(\omega_0 t-\beta_0 z)]+\text{c.c.}\ , \tag{2.1}$$

where $\hat{\mathbf{e}}$ is the polarization unit vector, $U(\rho)$ is the field distribution in the radial direction ρ of the single-mode supported by the fiber, $\beta_0 \equiv n(\omega_0)(\omega_0/c)$ is the propagation constant at the carrier frequency ω_0, and $A(z,t)$ is the amplitude of the pulse envelope. To account for the dispersive and nonlinear effects, the refractive index of the fiber medium is taken to be

$$\tilde{n}(\omega,|E|^2)=n(\omega)+n_2|E|^2\ , \tag{2.2}$$

where n_2 is the coefficient of the nonlinear index of refraction at the carrier frequency ω_0.

We substitute Eqs. (2.1) and (2.2) in the wave equation and integrate over the radial direction. Since the pulse spectrum is centered around ω_0, we expand the propagation constant $\beta(\omega)$ in a Taylor series about ω_0 and retain terms up to third order

$$\beta(\omega)=n(\omega)\frac{\omega}{c}=\beta_0+\beta_1(\omega-\omega_0)+\tfrac{1}{2}\beta_2(\omega-\omega_0)^2\ , \tag{2.3}$$

where $\beta_n=d^n\beta/d\omega^n$ is evaluated at the carrier frequency ω_0. If we introduce the reduced time

$$\tau=t-\beta_1 z\ , \tag{2.4}$$

and make the slowly-varying-envelope approximation, we obtain the following equation for the pulse-envelope amplitude:

$$i\left[\frac{\partial A}{\partial z}+\frac{1}{2}\alpha A\right]-\frac{1}{2}\beta_2\frac{\partial^2 A}{\partial\tau^2}+\gamma|A|^2A=0\ , \tag{2.5}$$

where α is the absorption coefficient and γ is the nonlinear coefficient given by

$$\gamma=\frac{n_2\omega_0}{c}\left[\int_0^\infty |U(\rho)|^4\rho\,d\rho\Big/\int_0^\infty |U(\rho)|^2\rho\,d\rho\right] . \tag{2.6}$$

For the lossless case ($\alpha=0$), Eq. (2.5) reduces to the nonlinear Schrödinger equation which allows for the solitons in the anomalous dispersion regime where the group-velocity dispersion $\beta_2<0$. To consider a realistic situation, we allow for the fiber loss and obtain numerical solutions of the following equation:

$$\frac{\partial A}{\partial z}=-\frac{1}{2}\alpha A+\frac{i}{2}\beta\frac{\partial^2 A}{\partial\tau^2}+i\gamma|A|^2A , \tag{2.7}$$

where, for simplicity of notation, we define $\beta=-\beta_2$ so that β is positive in the anomalous dispersion region of interest. Equation (2.7) is often written in normalized form.[1-4] However, we use this form to facilitate the comparison of the numerical results with experiments.

The numerical procedure is based on the Fourier-transform-based beam propagation technique.[19,20] More specifically, Eq. (2.7) is written formally as

$$\frac{\partial A}{\partial z}=(D+N)A , \tag{2.8}$$

where the differential operator D includes the first two terms involving loss and dispersion while N consists of the last nonlinear term. An exact solution of Eq. (2.8) is difficult to obtain because of the noncommutating nature of the operators D and N. However, an approximate solution, accurate to third order in step size δ, can be obtained using the following split-step procedure[19,20] to propagate the complex field:

$$A(z+\delta,\tau)=\exp\left[\frac{\delta D}{2}\right]\exp\left[\int_z^{z+\delta}N(z')dz'\right]\times\exp\left[\frac{\delta D}{2}\right]A(z,\tau) . \tag{2.9}$$

The numerical procedure consists of propagating the field by a distance $\delta/2$ with dispersion only, multiplying the result by a nonlinear term, and then propagating the field for the remaining distance $\delta/2$ with dispersion only. The propagation in the lossy, dispersive, but linear medium is accomplished using the Fourier-transform method. The integral in the nonlinear term in Eq. (2.9) is approximated by

$$\int_z^{z+\delta}N(z')dz'\simeq[N(z)+N(z+\delta)]\frac{\delta}{2} . \tag{2.10}$$

Note that $N(z+\delta)$ is not known while evaluating the integral at the midsegment located at $z+\delta/2$. We have followed an iterative approach that is initiated by replacing $N(z+\delta)$ with $N(z)$ in Eq. (2.10). Two iterations were found to be enough in practice.

III. MODULATION INSTABILITY

As mentioned in the Introduction, the propagation of a cw beam in fibers becomes unstable under certain conditions and may lead to its breakup into a train of short optical pulses. In this section we briefly consider the relevant features of the modulation instability needed later for our discussion of SAM. For simplicity, we consider the lossless case. The wave equation (2.7) with $\alpha=0$ becomes

$$\frac{\partial A}{\partial z}=\frac{i}{2}\beta\frac{\partial^2 A}{\partial\tau^2}+i\gamma|A|^2A . \tag{3.1}$$

The steady-state solution of Eq. (3.1) is given by

$$\bar{A}(z)=A_0\exp(i\gamma A_0^2 z) , \tag{3.2}$$

where A_0 is the incident amplitude of the cw beam.

To investigate the stability of the cw solution, we consider small perturbations around the steady state of the form

$$A(z,\tau)=[A_0+a(z,\tau)]\exp(i\gamma A_0^2 z) . \tag{3.3}$$

We substitute Eq. (3.3) in Eq. (3.1), linearize in $a(z,\tau)$, and assume a general solution of the form

$$a(z,\tau)=a_1\exp[i(Kz-\Omega\tau)]+a_2\exp[-i(Kz-\Omega\tau)] . \tag{3.4}$$

This procedure leads to the following dispersion relation:[12-16]

$$K=\pm\tfrac{1}{2}\beta\Omega(\Omega^2-\Omega_c^2)^{1/2} , \tag{3.5}$$

where

$$\Omega_c=(4\gamma A_0^2/\beta)^{1/2} . \tag{3.6}$$

For $|\Omega|<\Omega_c$, K is imaginary and the perturbation (3.4) grows exponentially with z. The cw solution is then unstable against small perturbations. This instability is referred to as modulation instability. The net power gain is obtained using

$$g=2\,\mathrm{Im}(K)=\beta\Omega(\Omega_c^2-\Omega^2)^{1/2} . \tag{3.7}$$

The gain is maximum at

$$\Omega_{\max}=\Omega_c/\sqrt{2} , \tag{3.8}$$

and has a value

$$g_{\max}=2\gamma A_0^2 . \tag{3.9}$$

In the presence of small fiber loss, an approximate expression for the gain has been obtained.[13]

Modulation instability can be interpreted in terms of a four-wave-mixing process. If a probe wave at the frequency $\omega_1=\omega_0+\Omega$ propagates with the cw beam, it experiences a net gain given by Eq. (3.7) as long as $|\Omega|<\Omega_c$. Physically, two photons from the intense beam at ω_0 are converted into two different photons, one at the probe frequency ω_1 and the other at the frequency

$2\omega_0-\omega_1$. Modulation instability has been observed[16] by launching such a weak probe pulse together with the intense pump pulse. In an earlier experiment,[15] modulation of the pulse envelope was observed without the use of a probe beam and was interpreted as arising from spontaneous emission. In the four-wave-mixing picture, the new frequency components are thought to build up from noise.

As is well known,[9-11] for optical pulses the phenomenon of SPM broadens the power spectrum as the pulses propagate inside the fiber. There is an additional mechanism that can generate the required frequency component without the use of an external probe or internal noise. SPM introduces new frequency components which can play the role of probe and lead to the process of four-wave mixing. When the loss is negligible and the initial condition is suitable, high-order solitons can result. Pulse-shape evolution has been studied numerically up to $N=3$.[21-23] These simulations show limited subpulse structure. However, our calculations extend well beyond $N=3$ and show much greater subpulse formation.

IV. RESULTS AND DISCUSSION

The evolution of the pulse profile and spectra along the fiber length is obtained by solving Eq. (2.7) numerically using the procedure outlined in Sec. II. The parameters for the initial numerical simulations are chosen to correspond to a realistic 1.55-μm optical communication system. In particular, $\alpha=0.046$ km^{-1} corresponds to a fiber loss of 0.2 dB/km and $\beta=20.4$ ps^2/km corresponds to a fiber dispersion of 16 ps/(km nm). The peak intensity A_0^2 can be written as $P/\bar{a}$, where P is the peak power and $\bar{a}$ is the area of the mode spot size in the fiber. The half width (σ) at which the intensity drops by $1/e$ is chosen to be 62.5 ps and corresponds to a full width at half maximum (FWHM) of about 100 ps for a Gaussian pulse. In addition it should be noted that since modulation instability corresponds to a cw beam, significant pulse narrowing ($\sigma \ll 100$ ps) may give rise to reduced agreement between modulation instability theory and experiments.

The incident field at the launch plane $z=0$ is taken to be[24]

$$A(0,\tau)=A_0\exp\left[-\frac{1}{2}\left[\frac{\tau}{\sigma}\right]\right]^{2m} . \tag{4.1}$$

The parameter m in Eq. (4.1) controls the pulse shape. For $m=1$, the pulse shape is Gaussian. For larger values of m we obtain the so-called super-Gaussian pulses[24] which become increasingly rectangular shaped as m increases. The parameter m can then be related to the rise time τ_r associated with the sharp leading and trailing edges of the pulse through the relation[24]

$$\tau_r \simeq \sigma/m . \tag{4.2}$$

In order to gain insight into the role played by nonlinearity and dispersion, the case of pure SPM (no dispersion, $\beta=0$) was studied. In the absence of dispersion the pulse shape does not change during propagation. Figure 1 compares the spectra with (solid curve) and without (dashed curve) dispersion for $z=0,4,8,12$ km. At $z=0$ and 4 km, the two spectra are identical. However at $z=8$ km, a new peak at the frequency $\nu\sim 45$ GHz occurs and at $z=12$ km the spectrum acquires several new peaks corresponding to higher harmonics. The appearance of this frequency component corresponds to a change in the pulse shape. Figure 2 shows the pulse shape at $z=12$ km which is modulated with a peak separation of ~ 15 ps and a pulse width of a few picoseconds. The occurrence of SAM is directly related to the appearance of the new frequency component in the power spectrum. We will refer to this frequency as the SAM frequency.

Next we describe experimental results. Using a Nd:YAG laser operating at 1.319 μm (where YAG represents yttrium aluminum garnet), we performed experiments on a 6.5-km length of monomode optical fiber. Since modulation instability occurs only in the anomalous dispersion region, a special fiber was fabricated having its zero-dispersion point at 1.29 μm resulting in dispersion of -2 ps^2/km at 1.319 μm and the fiber loss was 0.4 dB/km. The spectral features were studied using a computer controlled monochromator. Autocorrelation methods were used to study the pulse shape.

The pulse width (FWHM) of the laser was ~ 100 ps and the peak power was varied from 100 mW to several watts. At powers near a watt, stimulated Raman scattering dominated and details of the subpulse formation could not be obtained. At powers of about 200 mW, there was no noticeable pulse splitting, in agreement with numerical computations. However, by 350

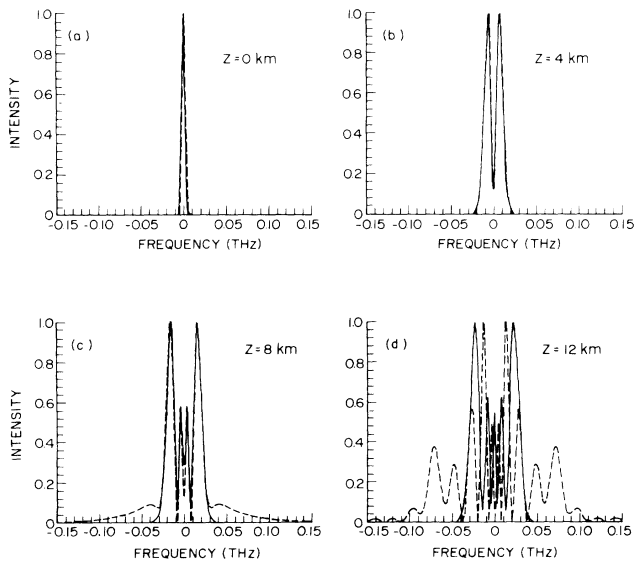

FIG. 1. Comparison of the spectra of a Gaussian pulse with (dashed curve) and without (solid curve) dispersion. Note the generation of new frequency components in the presence of dispersion.

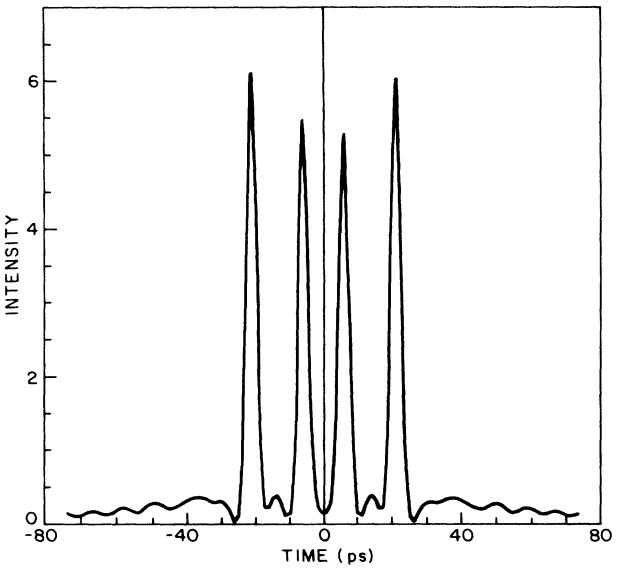

FIG. 2. Pulse shape at $z=12$ km under same conditions as Fig. 1.

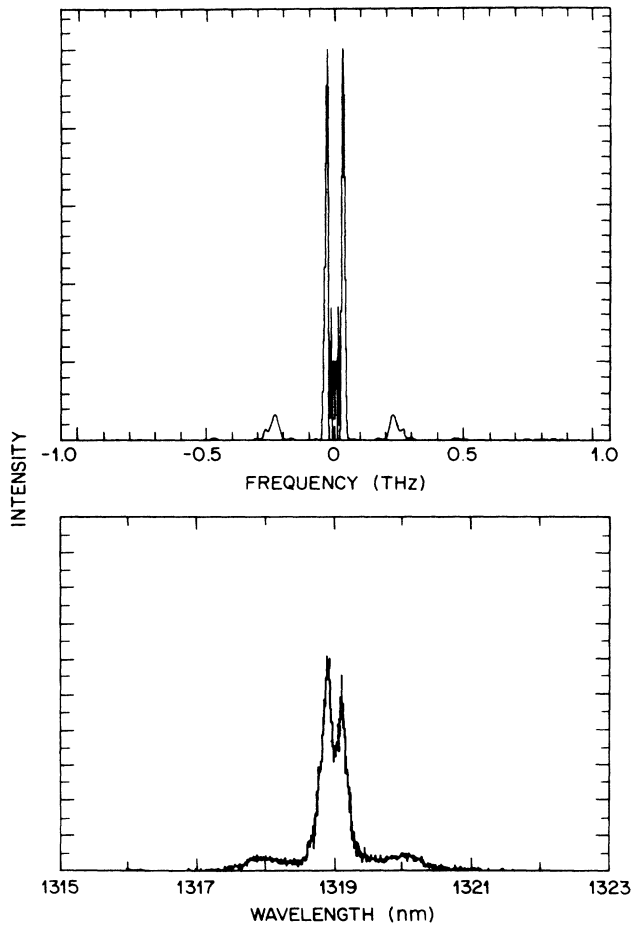

FIG. 3. Numerical (upper portion) and experimental (lower portion) spectra at 1.319 μm.

mW two new peaks have developed in the spectrum. The upper (lower) portion of Fig. 3 shows the numerical (experimental) spectrum. Numerical analysis shows that the central portions of the spectrum (-0.1 THz $<\nu<0.1$ THz) are due to self-phase-modulation, while the higher frequencies ($+0.23$ THz) are due to SAM. The qualitative feature of the numerical and experimental results are in reasonable agreement as seen from Fig. 3. The measured SAM frequency of 0.21 THz (1.2 nm) is in reasonable agreement with the numerical calculation. These numerical simulations do not contain any spontaneous emission or additional probe beams.

The power dependence of the SAM frequency and resultant subpulse formation can be understood qualitatively from Eq. (3.8), by writing $\nu_{\max}$ as

$$\nu_{\max}=\frac{\Omega_{\max}}{2\pi}=\frac{1}{2\pi}\left[\frac{2\gamma P}{\beta\bar{a}}\right]^{1/2}. \tag{4.3}$$

Figure 4 compares the prediction for $\nu_{\max}$ (solid line) of Eq. (4.3) with that obtained by numerical simulations (dashed line). The normalization frequency ν_0 (0.29 THz) corresponds to the power level of $P_0=350$ mW. The exact $P^{1/2}$ dependence of $\nu_{\max}$ predicted by the modulation instability holds only for cw operation. The dashed line, obtained for 100-ps-wide pulses, shows this dependence is approximately correct for low powers. At high power levels $\nu_{\max}$ is significantly lower for the pulsed operation than that obtained for cw operation. The experimental data points are in reasonable agreement with the numerical simulations.

Figure 5 shows the pulse shapes. Experimentally the

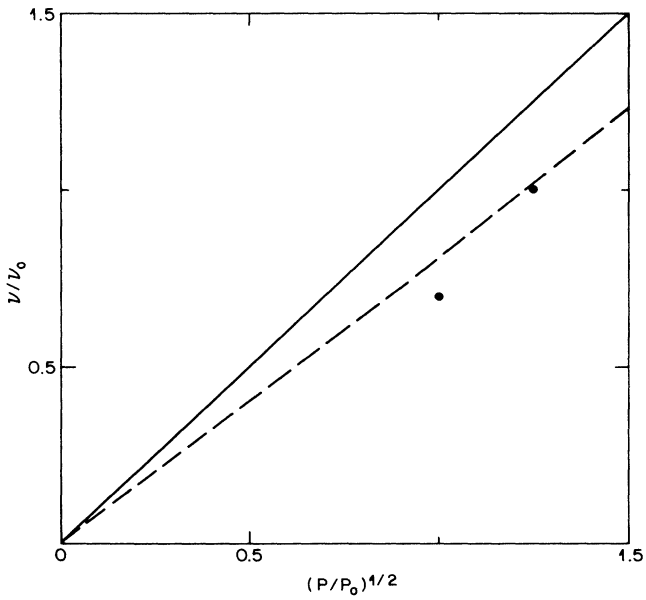

FIG. 4. Comparison of the values of $\nu_{\max}$ obtained from Eq. (4.3) (solid line) with those obtained by numerical calculations (dashed line). Dots indicate experimental data points.

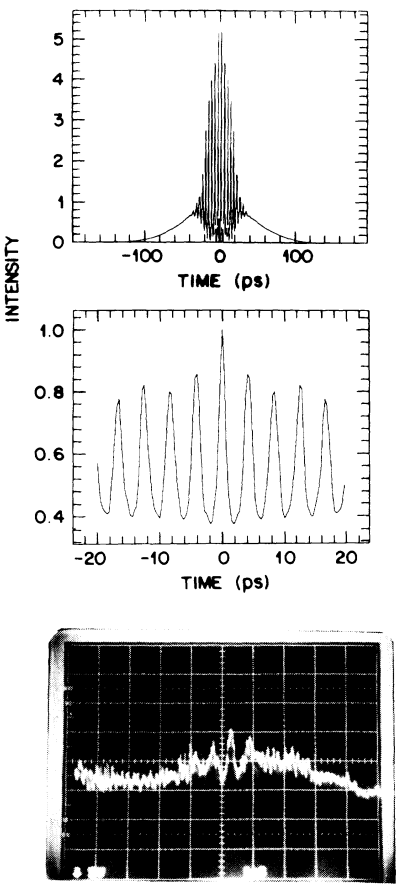

FIG. 5. Numerical calculations for the real-time (upper portion) and the autocorrelated (middle portion) shape profiles. Experimental results (lower portion) of the autocorrelated shape profile. The conditions are the same as in Fig. 3.

real time pulse could not be measured. Therefore the autocorrelation of the shape was measured and compared to numerical simulations. The upper (middle) portion of the figure shows the numerical results for the real-time (autocorrelated) shape profile. The measured autocorrelation of the shape profile is shown in the lower portion of the figure where the horizontal spacing is about 10 ps. While all of the details of the experimental autocorrelation could not be resolved, the experimental peak-to-peak separation of 5.5 ps is in reasonable agreement with the numerical result of 4.2 ps. The numerical autocorrelation shape is about 60% modulated similar to the experimental depth of modulation of about 50%. However, the upper portion of Fig. 5 shows that the central region of the real-time pulse shape is $\sim 100\%$ modulated. Our numerical results show that the experimental results can not arise solely from spontaneous emission, as previously believed.[15]

Finally, in order to study how SAM depends on the shape of the incident pulse, a super-Gaussian [$m=3$ in Eq. (4.1)] and a secant hyperbolic were investigated. The numerical calculations show that the resultant qualitative features of these shapes are similar to those of the Gaussian case. The similarity of the results for the three different pulse shapes suggests that the pulse shape does not play a significant role in the subpulse formation.

V. CONCLUSIONS

Motivated by previous measurements[15] showing a modulation developing in a temporally broad pulse, we performed numerical simulations of such behavior without the addition of spontaneous emission. The origin of the internal structure can be related to the modulation instability of continuous-wave optical beams in a nonlinear dispersive medium. However, it does not depend solely on spontaneous emission or an external probe for its initiation. Numerical results show that self-phase-modulation broadens the power spectrum enough to encompass the frequency at which modulation instability provides maximum gain. The pulse breakup may also be viewed as the internal structure of a high-order soliton, particularly if the fiber loss is neglected. From this point of view, it may be possible to obtain the details of the subpulse formation using the formalism of the inverse-scattering theory.[25–27] However, modulation instability appears to provide a simpler interpretation and is able to explain the features of numerical simulations and experiments.

[1]A. Hasegawa and F. Tappert, Appl. Phys. Lett. **23**, 142 (1973); A. Hasegawa and Y. Kodama, Proc. IEEE **69**, 1145 (1981).
[2]L. F. Mollenauer, R. H. Stolen, and J. P. Gordon, Phys. Rev. Lett. **15**, 1095 (1980); R. H. Stolen, L. F. Mollenauer, and W. J. Tomlinson, Opt. Lett. **8**, 186 (1983).
[3]L. Mollenauer, J. P. Gordon, and M. N. Islam, IEEE J. Quantum Electron. **QE-22**, 157 (1986).
[4]N. J. Doran and K. J. Blow, IEEE J. Quantum Electron. **QE-19**, 1883 (1983); K. J. Blow, N. J. Doran, and B. P. Nelson, Opt. Lett. **10**, 393 (1985).
[5]D. Anderson, Phys. Rev. A **27**, 3135 (1985); Proc. Inst. Electr. Eng. Part 1, **132**, 122 (1985).
[6]M. J. Potasek, G. P. Agrawal, and S. C. Pinault, J. Opt. Soc. Am. B **3**, 205 (1986).
[7]G. P. Agrawal and M. J. Potasek, Phys. Rev. A **33**, 1765 (1986).
[8]B. Nikolaus and D. Grischkowsky, Appl. Phys. Lett. **42**, 1 (1983); **43**, 228 (1983).
[9]W. J. Tomlinson, R. H. Stolen, and C. V. Shank, J. Opt. Soc. Am. B **1**, 139 (1984).
[10]K. Tai and A. Tomita, Appl. Phys. Lett. **48**, 309 (1986).
[11]A. Hasegawa and W. F. Brinkman, IEEE J. Quantum Electron. **QE-16**, 694 (1980).
[12]A. Hasegawa, Opt. Lett. **9**, 288 (1984).
[13]D. Anderson and M. Lisak, Opt. Lett. **9**, 468 (1984).
[14]P. K. Shukla and J. Juul Rasmussen, Opt. Lett. **11**, 171 (1986).
[15]K. Tai, A. Tomita, and A. Hasegawa, Phys. Rev. Lett. **56**,

135 (1986).
[16]K. Tai, A. Tomita, J. L. Jewell, and A. Hasegawa, Appl. Phys. Lett. **49**, 236 (1986).
[17]J. A. Fleck, J. R. Morris, and M. D. Feit, Appl. Phys. **10**, 129 (1976).
[18]M. J. Potasek, Opt. Lett. **12**, 717 (1987).
[19]M. Lax, J. H. Batteh, and G. P. Agrawal, J. Appl. Phys. **52**, 109 (1981).
[20]G. P. Agrawal, J. Appl. Phys. **56**, 3100 (1984).
[21]K. J. Blow, N. J. Doran, and E. Cummins, Opt. Commun. **48**, 181 (1983).
[22]L. F. Mollenauer, R. H. Stolen, J. P. Gordon, and W. J. Tomlinson, Opt. Lett. **8**, 289 (1983).
[23]D. Yevick and B. Hermansson, Opt. Commun. **47**, 101 (1983).
[24]G. P. Agrawal and M. J. Potasek, Opt. Lett. **11**, 318 (1986).
[25]C. S. Gardner, J. M. Greene, M. D. Kruskal, and R. M. Miura, Phys. Rev. Lett. **19**, 1095 (1967).
[26]V. E. Zakharov and A. B. Shabat, Zh. Eksp. Teor. Fiz. **61**, 118 (1971) [Sov. Phys.—JETP **34**, 62 (1972)].
[27]J. Satsuma and N. Yajima, Prog. Theor. Phys. Suppl. **55**, 284 (1974).

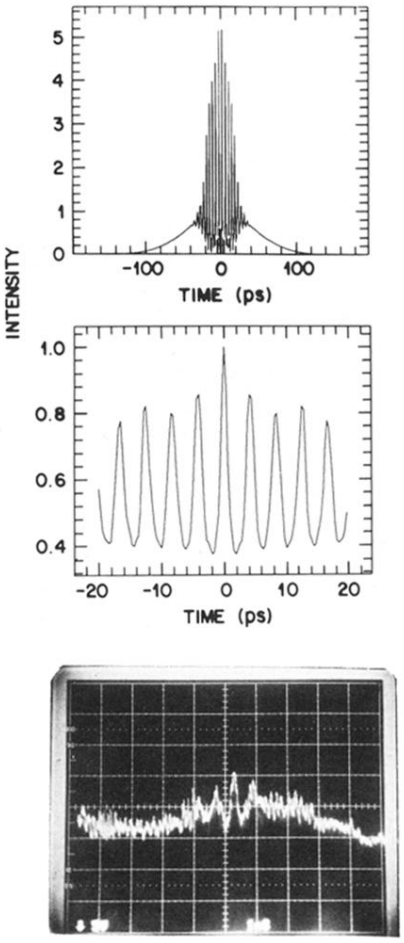

FIG. 5. Numerical calculations for the real-time (upper portion) and the autocorrelated (middle portion) shape profiles. Experimental results (lower portion) of the autocorrelated shape profile. The conditions are the same as in Fig. 3.